Journal of Membrane Science 513 (2016) 226–235

Contents lists available at ScienceDirect

Journal of Membrane Science

journal homepage: www.elsevier.com/locate/memsci

Direct incorporation of silver nanoparticles onto thin-film composite membranes *via* arc plasma deposition for enhanced antibacterial and permeation performance

Sang-Hee Park [a,1], Sang Hoon Kim [b,1], Sung-Joon Park [a,1], Sungmin Ryoo [c], Kyoungja Woo [c], Jong Suk Lee [d], Taek-Seung Kim [e], Hee-Deung Park [e], Hosik Park [f], You-In Park [f], Jinhan Cho [a], Jung-Hyun Lee [a,*]

[a] Department of Chemical and Biological Engineering, Korea University, 5-1 Anam-dong, Seongbuk-gu, Seoul 136-713, Republic of Korea
[b] Materials Architecturing Research Center, Korea Institute of Science and Technology, 39-1 Hawolgok-dong, Seongbuk-gu, Seoul 136-791, Republic of Korea
[c] Nanophotonics Research Center, Korea Institute of Science and Technology, 39-1 Hawolgok-dong, Seongbuk-gu, Seoul 136-791, Republic of Korea
[d] Center for Environment, Health and Welfare Research, Korea Institute of Science and Technology, 39-1 Hawolgok-dong, Seongbuk-gu, Seoul 136-791, Republic of Korea
[e] Department of Civil, Envrionmental Engineering and Archirtectural Engineering, Korea University, 5-1 Anam-dong, Seongbuk-gu, Seoul 136-713, Republic of Korea
[f] Advanced Materials Division, Center for Membranes, Korea Research Institute of Chemical Technology, Yuseong-gu, Daejeon, 305-600, Republic of Korea

ARTICLE INFO

Article history:
Received 15 October 2015
Received in revised form
10 February 2016
Accepted 5 April 2016
Available online 14 April 2016

Keywords:
Silver nanoparticle
Polyamide thin film composite membrane
Antibacterial property
Biofouling
Arc plasma deposition

ABSTRACT

We report on a new technique that incorporates silver nanoparticles (AgNPs) onto polyamide (PA) thin film composite (TFC) reverse osmosis membranes *via* arc plasma deposition (APD) to impart antibacterial properties and simultaneously improve membrane performance. APD allows the direct deposition of AgNPs under vacuum dry condition, overcoming the drawbacks of the conventional wet-chemical methods. AgNPs (~7.6 nm in diameter) were uniformly distributed without aggregation throughout the PA selective layer with some partially implanted into the PA matrix. Ag loading could be tuned by simply adjusting the number of APD purse shots. The deposited AgNPs exhibited good leaching stability, presumably due to the strong Ag-PA chemical interaction and partially buried AgNP morphology. The resulting Ag-incorporated TFC (Ag-TFC) membrane showed the strong and long-lasting antibacterial properties for both gram-negative and -positive bacteria. Simultaneously, the Ag-TFC membrane exhibited an enhancement in water flux of approximately 40% without deterioration in NaCl rejection. These performance changes were tentatively attributed to the partial destruction of the PA layer under the high energetic APD condition along with the increased membrane hydrophilicity. Hence, the APD process provides a simple and effective route to modify membranes with functional NPs.

1. Introduction

Membrane-based reverse osmosis (RO) and nanofiltration (NF) processes are the most energy-efficient technologies for desalination, water purification and wastewater treatment [1,2]. Polyamide (PA) thin film composite (TFC) membranes are commonly used commercially as RO and NF membranes due to their high permselectivity and wide-range pH stability [1,2]. However, the widespread application of PA TFC membranes has been hampered by biofouling, which is caused by the undesirable attachment of bacteria or microorganisms and their subsequent growth into a biofilm. Membrane biofouling adversely affects membrane performance by decreasing water permeability, leading to increased energy consumption and operational costs of membrane processes [2,3].

Conventionally biofouling is prevented by using disinfectants such as chlorine, but such methods are often unsatisfactory because bacteria cannot be completely inactivated by disinfectant treatment alone and the survived bacteria can grow and multiply. In addition, the prolonged exposure of membranes to disinfectants can lead to the structural damage and performance deterioration of PA TFC membranes [4]. Hence, many attempts have been made to improve membrane biofouling resistance including the surface functionalization and modification of the membrane with various

* Corresponding author. Tel.: +82 2 3290 3293; fax: +82 2 926 6102.
E-mail address: leejhyyy@korea.ac.kr (J.-H. Lee).
[1] These authors contributed equally.

http://dx.doi.org/10.1016/j.memsci.2016.04.013
0376-7388/

nanomaterials [5–8]. In particular, the incorporation of biocidal nanomaterials into TFC membranes has been recognized as a promising approach to alleviate biofouling. Such nanomaterials include silver (Ag) [9–15], copper [16] and titanium oxide nanoparticles (NPs) [17,18], graphene oxide [7] and enzymes [19]. Among them, AgNPs have been extensively explored as the most attractive antibacterial material owing to their strong and broad-spectrum biocidal effect and low human cytotoxicity [20,21]. Recent efforts have been devoted to devising a more effective method to incorporate AgNPs into the membranes including physical adsorption, covalent binding, layer-by-layer coating and *in-situ* incorporation. Although the methods reported to date have proven to effectively impart the antibacterial properties to the membranes and thereby mitigate membrane biofouling, there remain several technical issues to be addressed. First, most of the proposed methods rely on wet-chemical routes and their inevitable discharge of chemical wastes such as residual solvents, chemicals and AgNPs not only causes environmental and health concerns but also increases processing cost. Second, many of the techniques have multiple sequential reaction steps, making the process time- and cost-consuming [12,13]. Third, some methods excessively overuse AgNPs, causing their antibacterial activity to be adversely affected by their aggregation, which is facilitated by their small particle size [22]. Although modification of NPs with capping agents may enhance the NP dispersion, it also typically reduces the antibacterial activity and immobilization efficiency of NPs by the interference of the organic materials present on their surface [23]. Finally, the incorporation processes often led to deterioration in membrane performance, in terms of salt rejection and/or water flux, due to membrane damage and/or increased hydrodynamic resistance during the process [9,10,12–15]. These drawbacks motivate the continued search for more simple and effective NP incorporation methods.

Arc plasma deposition (APD) is one of physical vapor deposition techniques, in which highly ionized metal ions are released from a metal cathode by generating arc pulse plasma, and then deposited on a substrate with high kinetic energy to be condensed to NPs [24–26]. In the field of material and surface engineering, APD has been widely used to fabricate functional films and coatings through the deposition of various metal and ceramic NPs. Their size and loading can be precisely controlled by adjusting the magnitude of the arc voltage and the number of arc pulses and NPs can be uniformly distributed [25,26]. In addition, the APD process offers the following key potential merits: (1) good NP-substrate adhesion (2) fast deposition rate and (3) high reliability. Hence, APD is a direct and simple dry method for the deposition of functional NPs, which can overcome the aforementioned shortcomings of conventional wet-chemical methods. Despite the many advantages of the APD method, no attempt has yet been made to apply it to the incorporation of NPs onto membranes.

In this study, for the first time, we employed an APD process to incorporate AgNPs onto a PA TFC RO membrane for imparting the antibacterial properties and simultaneously improving membrane performance. APD allows the direct, uniform and robust deposition of AgNPs over the entire PA selective layer. The Ag loading was controlled by adjusting the number of arc pulse shots. The structures and physicochemical properties of the AgNP-incorporated TFC (Ag-TFC) membranes were comprehensively characterized. The Ag-TFC membranes exhibited strong antibacterial properties for both gram-negative and -positive bacteria. Importantly, the key merit of APD is that, by controlling APD deposition, the water permeability of the membrane could be greatly enhanced without compromising NaCl rejection. The deposited AgNPs showed a relatively slow releasing rate of Ag^+ ions along with the good stability against the detachment. Plausible explanations for the improved membrane performance and the good NP stability obtained through APD modification were discussed.

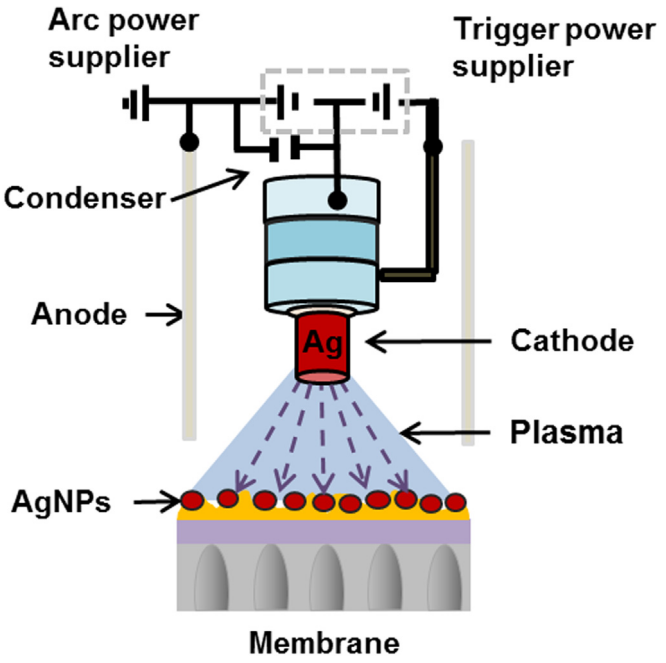

Fig. 1. Schematic illustration of the direct deposition of AgNPs onto a TFC membrane *via* APD.

2. Experimental

2.1. Materials

A commercial PA TFC RO membrane (SWC4+) was obtained from Nitto Denko. Sodium chloride (NaCl, Junsei Chemical Co.), phosphate buffered saline (PBS, Sigma-Aldrich), Luria-Bertani (LB) broth miller (BD Difco™) and agar (extra pure, Daejung Chemical Co.) were used as purchased. Deionized (DI) water (18.2 MΩ cm) was prepared in a Millipore Milli-Q purification system. *Escherichia coli* (*E. coli*, ATCC 47,076) was obtained from the American Type Culture Collection. *Pseudomonas aeruginosa* (*P. aeruginosa*, KCTC 2004) and *Staphylococcus aureus* (*S. aureus*, KCTC 3881) were received from the Korean Collection for Type Cultures.

2.2. APD deposition

AgNPs were directly deposited onto the commercial RO membrane (6×6 cm^2 in size) by a coaxial arc pulse deposition (APD) system (ULVAC, ARL-300) at room temperature under a vacuum (10^{-5} Torr), as depicted in Fig. 1. A cathode rod made of target Ag is located at the center and a cylindrical anode is coaxially placed in the APD system. A condenser stores a certain amount of charge, which is discharged from a cathode to an anode *via* an arc over a short time period (≤ 1 ms) induced by a trigger pulse. This discharge process rapidly heats up the Ag cathode spot to more than tens of thousands of °C, which vaporizes the cathode material to generate an ionized Ag plasma pulse. Under the strong magnetic field, the released Ag plasma ions move with high kinetic energies (20–200 eV), collide with the membrane surface and are deposited and condensed as nanoparticles. This process could result in the physical implantation of AgNPs into the membrane network. Right after discharging, the condenser rapidly returns to the charged state and is then ready to generate the next plasma pulse. The Ag loading was controlled by adjusting the number of plasma arc

pulse shots (10 – 100) while keeping the discharge condenser voltage (85 V), the discharge condenser capacity (1080 μF) and plasma pulse frequency (1 Hz) constant.

2.3. Membrane characterization

The surface morphologies of the pristine and Ag-deposited TFC membranes (Ag-TFC) were characterized by scanning electron microscopy (SEM, FEI Inspect F50). The cross-sectional morphology of the Ag-TFC membrane was examined with transmission electron microscopy (TEM, FEI Tecnai F20 G2) to characterize the size, shape and spatial distribution of the deposited AgNPs. To prepare the TEM sample, the polyester fabric backing was first peeled off from the TFC membrane, and the sample was embedded in epoxy resin (Polybed 812), followed by curing at 60 °C for 24 h. Then, the sample was cut on an ultra-microtome (Reichert UltracutS) and mounted onto a copper grid. The cross-sections were imaged at an accelerating voltage of 200 kV. The chemical composition of the membrane was characterized by X-ray photoelectron spectroscopy (XPS, PHI 5000 VersaProbe, Physical electronics, Inc.) using monochromatized Al K_α radiation at 1486.6 eV to confirm the deposition of Ag and identify the chemical state of the deposited Ag. The water contact angles were measured by the sessile drop method using a goniometer (KSV CAM 200 goniometer, KSV Instruments) equipped with a video capture camera. For each sample at least five measurements were taken at different locations to obtain the averaged contact angle value. The resistance of AgNPs to leaching from the Ag-TFC membrane was evaluated by monitoring changes in both the Ag content of the membrane, using XPS, and the membrane surface morphology after either sonication (power = 70 W, frequency = 20 kHz) for 3 min or a RO performance test with DI water (flow rate = 1 L min^{-1}, an operating pressure = 15.5 bar) for 24 h.

2.4. Membrane performance evaluation

The membrane performance (water flux and NaCl salt rejection) was evaluated with a lab-scale cross-flow filtration system with an effective membrane area (A) of 12.4 cm^2. The filtration test was performed with an aqueous feed solution of 2000 ppm NaCl (pH = 5.8) at a flow rate of 1 L min^{-1}, an operating pressure of 15.5 bar and an operating temperature of 25 °C. Water flux (J_w, L m^{-2} h^{-1}, LMH) was calculated from the amount of the permeate (V) collected over the time interval (t) using the equation, $J_w = V/At$. NaCl salt rejection (R, %) was determined from the NaCl concentrations of the feed (C_f) and permeate solutions (C_p), measured with a conductivity meter (Ultrameter II, Myron L. Company) using the equation as given by $R = (C_f - C_p)/C_p \times 100$.

2.5. Antibacterial activity assessment

The antibacterial properties of the membranes were assessed for three model bacterial stains (*E. coli*, *P. aeruginosa* and *S. aureus*) following the protocol reported in the literature [27,28]. Bacteria were cultivated in LB at 37 °C overnight with shaking. The cultures were diluted with fresh LB broth, followed by further incubation for 3 h. The bacterial cells were separated from the broth by the centrifugation, and then re-suspended in 10 mM PBS solution (pH = 7.4). All bacterial solutions were diluted to 10^6 colony forming units (CFU) mL^{-1}. Next, a 4 cm^2 membrane coupon was soaked into the prepared bacterial solution, and subsequently incubated at 37 °C for 2 h. The membrane coupon was then removed from the bacterial solution. The remaining supernatant was diluted and then spread on LB agar plates which had been prepared from LB broth miller (2.5 g in 100 mL DI water) and agar (2.0 g in 100 mL DI water), followed by incubation at 37 °C for 24 h. The number of colonies on each plate was counted to calculate the percent bacterial viability using the equation, bacterial viability (%) = $100 \times N/N_0$, where N and N_0 are the number of colonies of the bacterial cultures contacted with and without membranes, respectively.

Live and dead bacteria on the membrane surface were also identified by fluorescence microcopy [28]. After incubation at 37 °C for 2 h, the membrane was removed from the bacterial solution and then carefully washed with a PBS solution to remove the physically attached bacteria from the membrane surface. Subsequently, the membrane sample was stained with SYTO 9 and propidium iodide of the Live/Dead *Bac*Light bacterial viability kit (Molecular Probes, Willow Creek, OR, USA) for 15 min The stained membrane was washed twice with a PBS solution to remove loosely-bound dyes. The membrane surface was examined using confocal laser scanning microscopy (CLSM) (Carl Zeiss LSM700, Jena, Germany) with fluorescent filters having specific excitation and emission wavelengths (SYTO 9: 480 and 500 nm; PI: 490 and 635 nm). CLSM images were obtained using a 40 × objective lens (C-APOCHROMAT/1.20 W Korr M27, Carl Zeiss) and analyzed by the Zen 2012 program (Carl Zeiss).

2.6. Evaluation of the releasing rate of Ag^+ ions from the Ag-TFC membrane

The releasing rate of Ag^+ ions from the Ag-TFC membrane was also evaluated following the protocol reported by other researchers [12]. The 4 cm^2 Ag-TFC membrane coupon was soaked into 20 mL of DI water at 25 °C and then agitated at 50 rpm. The solution was replaced with fresh DI water every 24 h. All the collected solutions were acidified by 1 wt% HNO_3 aqueous solution and then analyzed by inductively coupled plasma mass spectrometer (ICP-MS, NEXION 300D, PerkinElmer) to quantify the amount of Ag dissolved in the collected solutions. Another Ag-TFC membrane coupon was soaked into 1 wt% HNO_3 aqueous solution while sonicating for 20 min to completely dissolve all the AgNPs present on the membrane. The total amount of Ag deposited onto the Ag-TFC membrane was determined by ICP-MS.

3. Results and discussion

3.1. Membrane characterization

Fig. 2a and b present the surface morphologies of the pristine and Ag-deposited (Ag-TFC, prepared by 40 APD pulse shots) membranes, respectively. The PA TFC membrane exhibits the ridge-and-valley surface structure typical of the cross-linked fully aromatic PA prepared *via* interfacial polymerization [1]. It can be seen from Fig. 2b that AgNPs are uniformly distributed over the entire membrane surface without aggregation. Further information of the structure and spatial distribution of AgNPs was provided by the cross-sectional TEM image of the Ag-TFC membrane, in which the AgNPs appear as dark spots (Fig. 2c). The deposited AgNPs are spherical in shape with an average diameter of $\sim 7.6 \pm 6.1$ nm. Consistent with the SEM observation, AgNPs appear uniformly distributed throughout the entire PA selective layer and no particle aggregates are visible. The uniform deposition of pristine, uncapped NPs highlights the advantage of the proposed APD technique over conventional wet-chemical methods in which the formation of NP aggregates is inevitable in the absence of the capping agents on the NP surface. Interestingly, the cross-sectional TEM image reveals that although many AgNPs are present on the surface, some (as denoted by red arrows in Fig. 2c) are buried within the PA selective layer, showing that they partially penetrated into the PA polymer matrix during APD. It is reasonable to

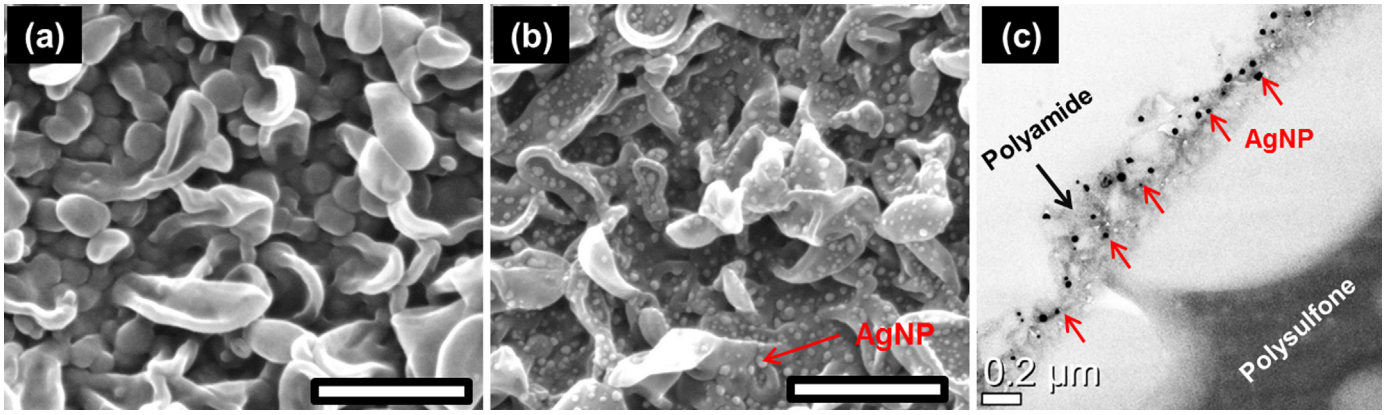

Fig. 2. (a and b) SEM surface images of (a) the pristine TFC and (b) Ag-TFC membranes (scale bar=500 nm). (c) Cross-sectional TEM image of the Ag-TFC membranes. The Ag-TFC membrane is prepared with 40 APD pulse shots. (For interpretation of the references to color in this figure, the reader is referred to the web version of this article.)

postulate that the high kinetic energy (20–200 eV) of plasma Ag ions generated during the APD process enhances ion mobility on the surface, causing the partial diffusion of NPs into the PA network [24,25]. The partial buried morphology of NPs is expected to enhance the NP stability against leaching.

The presence of AgNPs on the Ag-TFC membrane was further confirmed by the high resolution XPS spectrum of Ag, where there are two intense peaks at 368.5 and 374.5 eV corresponding to Ag $3d_{5/2}$, and Ag $3d_{3/2}$ cores, respectively, as shown in Fig. 3a. To identify the chemical state of the deposited AgNPs, Ag $3d_{5/2}$ peak was deconvoluted into three component peaks at 368.6, 368.1 and 367.5 eV, which correspond to Ag°, Ag^{+}, and Ag^{2+} states, respectively [11,29]. This reveals that the Ag deposited by APD is the mixture of metallic Ag and Ag oxides (Ag_2O and AgO) with approximately 85% being in the metallic state [11,29]. It is believed that, after APD, the Ag surface is oxidized to form a thin Ag oxide layer when it is exposed to ambient air [9]. As shown in Fig. 3b, the Ag content of the Ag-TFC membrane estimated from XPS increased continuously with increasing the number of APD plasma pulse shots. This result suggests that the Ag loading can be simply and precisely controlled by adjusting the number of plasma pulse shots for the APD process.

Membrane hydrophilicity was evaluated by measuring water contact angle since it is one of important membrane properties governing membrane performance and fouling behavior. Fig. 3c shows the water contact angle of the Ag-TFC membranes as a function of the number of APD pulse shots. The pristine TFC membrane (corresponding to 0 pulse shot) exhibited a water contact angle of $53.7 \pm 5.0^{\circ}$. Increasing the number of pulse shots, thereby increasing Ag loading, resulted in a reduction in the water contact angle, that is, increased membrane hydrophilicity. This result is consistent with the previous reports by other researchers who have observed that the incorporation of AgNPs increased the hydrophilicity of PA TFC membranes [11,12,30]. Enhanced membrane hydrophilicity with increasing Ag loading is attributed to the presence of the hydrophilic Ag oxide layer on the AgNP surface, as confirmed by the high resolution XPS analysis. A more hydrophilic surface would both enhance water permeation by increasing water solubility in the membrane and improve biofouling resistance by decreasing bacterial adhesion [6,31].

The stability of the AgNPs against detachment from the membrane was evaluated by monitoring changes in the surface morphology and XPS Ag content of the membrane before and after sonication for 3 min and the cross-flow RO filtration test with DI water for 24 h. The Ag-TFC membrane prepared with 100 pulse shots was selected as a control because it can maximize any changes in the Ag loading in response to operating conditions. Most AgNPs appeared to remain on the membrane surface after sonication (Fig. 4b), indicating a fairly strong binding of the AgNPs to the membrane surface. However, some of the AgNPs seem to be lost along with showing a reduction in the average AgNP size after the RO filtration test (Fig. 4c), presumably due to the detachment of a few of the weakly-bound AgNPs and the accelerated dissolution of AgNPs exposed to highly-pressurized shear flow conditions,

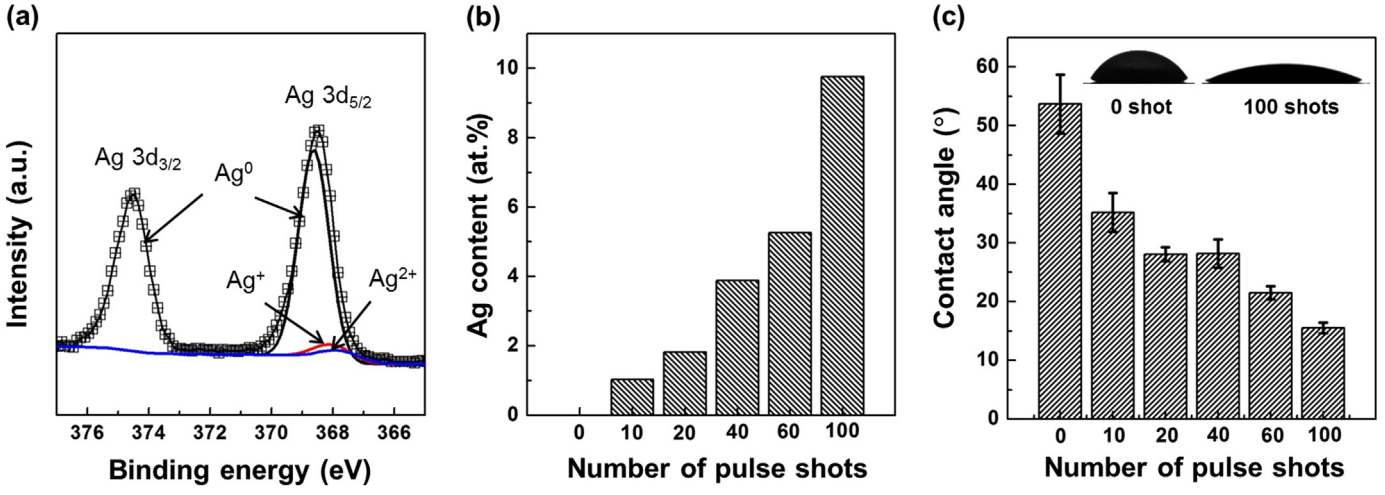

Fig. 3. (a) High resolution XPS spectra of the Ag peak for the Ag-TFC membrane (prepared with 40 APD pulse shots). (b) Ag content and (c) water contact angle of the Ag-TFC membrane as a function of APD pulse shots.

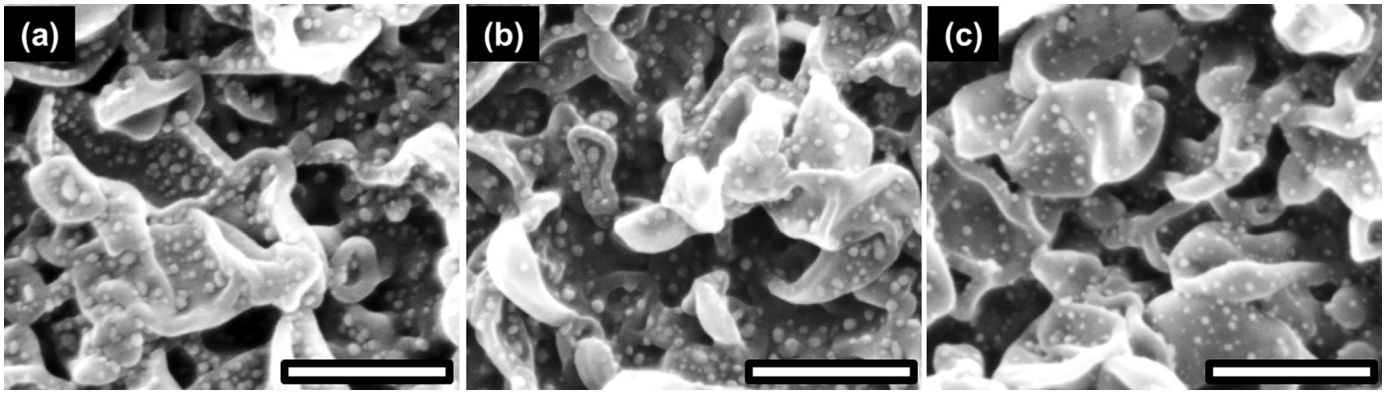

Fig. 4. SEM surface images of the Ag-TFC membranes (a) before treatment (b) after sonication and (c) after filtration. The Ag-TFC membrane is prepared with 100 APD pulse shots. The scale bar is 300 nm.

Table 1
Atomic content percentage (%) of carbon (C), nitrogen (N), oxygen (O) and silver (Ag) of the Ag-TFC membrane (prepared with 100 APD pulse shots).

	C	N	O	Ag
Before treatment	64.78	6.38	19.08	9.76
After sonication	64.85	6.78	19.39	8.98
After filtration	65.01	7.96	20.26	6.77

which remains to be addressed.

The composition analysis by XPS provides quantitative information on AgNP stability as presented in Table, 1. The Ag content of the membrane decreased by approximately 8% and 30% after sonication and filtration test, respectively, in qualitative agreement with the surface SEM examination. These relatively minor reductions in Ag content, despite the inherent and unavoidable oxidative loss of AgNPs upon their exposure to water, indicate that the Ag-TFC membrane has relatively good AgNP stability. The good resistance of AgNPs to leaching is attributed in part to the strong affinity of AgNPs with the PA matrix. Pakiari et al. reported that Ag strongly interacts with amino acids *via* forming two types of bonds: (1) the conventional anchoring N–Ag and O–Ag bonds and (2) the unconventional N–H···Ag and O–H···Ag hydrogen bonds [32]. Furthermore, several researchers have revealed a strong chemical interaction between the AgNP surface and carboxyl groups through surface-enhanced Raman scattering studies [33,34]. Based on the literature, one would expect AgNPs to be strongly bound to the PA selective layer of the TFC membrane *via* specific chemical interactions and hydrogen bonding since PA contains uncrosslinked amine and carboxyl moieties in addition to crosslinked amide groups. Moreover, the partially implanted morphology of the AgNPs within the PA matrix resulting from the high energetic deposition conditions during APD could provide an enhanced adhesion, which further augments AgNP leaching resistance [24].

3.2. Membrane performance

Fig. 5a represents the water flux and NaCl rejection of the Ag-TFC membranes as a function of the number of APD pulse shots. The pristine TFC membrane (corresponding to 0 pulse shot) has a water flux of 27.1 ± 1.0 L m^{-2} h^{-1} and NaCl rejection of 98.8 ± 0.5%, below the manufacturer's specification. Most lab-scale studies reported the NaCl rejection values of commercial membranes as being lower than those reported by the manufacturers due to differences in test conditions and protocols between the laboratory and the manufacturer [35]. As the number of pulse shots increases, NaCl rejection remained unchanged up to 60 shots (NaCl rejection = 98.9 ± 0.2%) but slightly decreased for 100 shots (NaCl rejection = 97.8 ± 0.8%). In other words, moderate APD conditions, with the number of APD pulse shots ≤ 60, did not deteriorate membrane selectivity. Interestingly, water flux rapidly increased up to 20 pulse shots and then gradually increased with increasing the number of pulse shots. As a result, compared to the pristine membrane, the Ag-TFC membrane prepared with 60 pulse shots exhibited a 40% enhancement in water flux (38.2 ± 0.4 L m^{-2} h^{-1}) and essentially the same NaCl rejection, demonstrating a further valuable advantage of the APD technique.

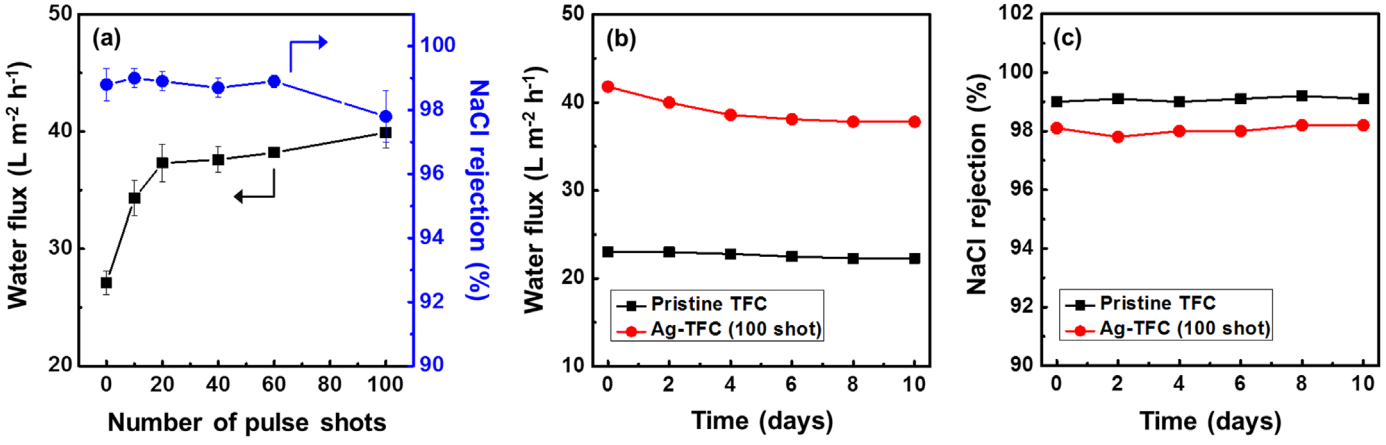

Fig. 5. (a) Water flux and NaCl rejection of the Ag-TFC membrane as a function of APD pulse shots. (b) water flux and (c) NaCl rejection of the pristine TFC and Ag-TFC (made with 100 APD pulse shots) membranes monitored during the long-term filtration test for 10 days.

Improved water flux could be connected to the increased hydrophilicity of the membrane by AgNP deposition as evidenced by water contact angle measurement [36,37]. However, it is hard to accept that the enhanced hydrophilicity alone can account for such a remarkable increase in water flux. Another plausible mechanism of the observed flux enhancement could be the structural alteration of the PA selective layer caused during the APD process. It has been widely recognized that the PA selective layer structure of TFC RO membrane is depth-heterogeneous as referred to as a sandwiched structure where the dense core PA layer determining the ion selectivity is positioned between the loose outmost PA sublayers [38–40]. The penetration of AgNPs into the PA layer during APD is believed to partially and preferentially destroy the topmost PA layer network and increase the flexibility of the PA chain, thereby facilitating the passage of water molecules across the membrane, while leaving the dense core selective layer intact. This hypothesis could account for the improved water flux with unchanged salt rejection for 60 or less pulse shots. A similar argument was used to explain the improvement in water flux without sacrificing salt selectivity for the graphene oxide-coated PA TFC membranes upon chlorine-induced oxidation, which presumably caused preferential destruction of the outmost PA layer [41]. However, an excessive pulsing condition (100 pulse shots) is likely to destruct the inner core PA region to some degree, resulting in a slight decline in NaCl rejection. Again, it should be noted that the common wet-chemical routes for membrane modification with

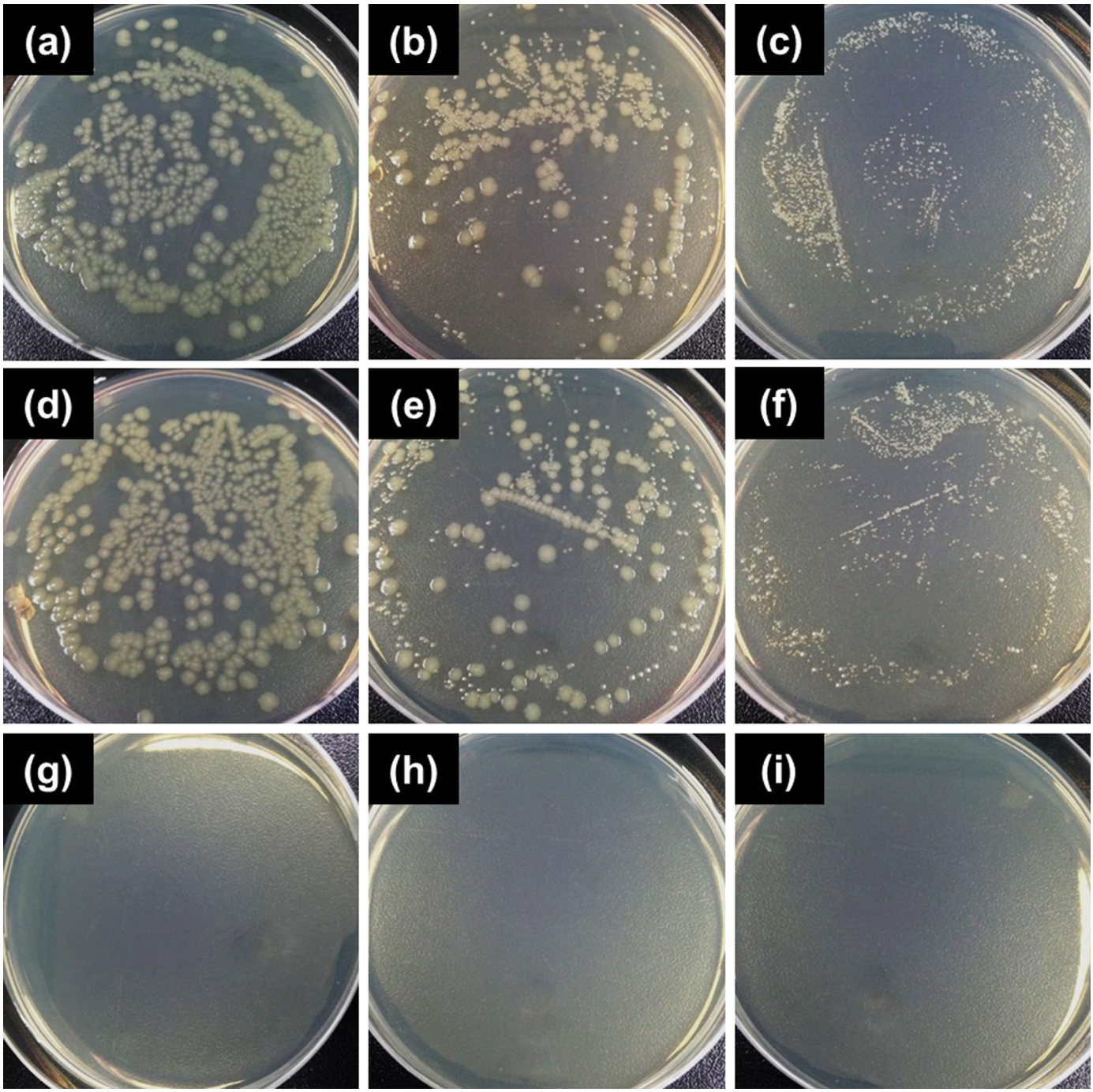

Fig. 6. Photographs of the bacterial culture plates of (a, d, g) *E. coli*, (b, e, h) *P. aeruginosa* and (c, f, i) *S. aureus* for the (a–c) control, (d–f) pristine TFC membranes and (g–i) Ag-TFC membranes. Control denotes the bacterial culture which has not had membrane contact. The Ag-TFC membrane is prepared with 40 APD pulse shots.

NPs relying on coating, grafting and *in-situ* incorporation often led to deterioration in membrane performance (water flux, rejection) [9,10,12–15]. Improvements in flux achieved by controlling APD conditions when functionalizing TFC membranes with NPs demonstrate the promising potential of the APD technique.

The membrane performances of the pristine TFC and Ag-TFC membranes (made with 100 APD pulse shots) were monitored during a cross-flow test for 10 days to see whether the performance alteration by APD modification is permanent as shown in Fig. 5b and c. Results showed that both water flux and NaCl rejection of the pristine TFC membrane were essentially unchanged during the test. For the Ag-TFC membrane, water flux slightly decreased by ~9.5%, while salt rejection remained almost unchanged for 10 days. Energy-disperse X-ray spectroscopy analysis on the Ag-TFC membranes before and after long-term filtration test revealed that Ag of approximately 70% was lost for 10 days. This result indicates that the loss of Ag does not significantly affect the separation performance of the Ag-TFC membrane. A minor rejection of ~9.5% in water flux of the Ag-TFC membrane after 10 day-filtration can be explained presumably by the decreased hydrophilicity resulting from the loss of Ag. Hence, the ultimate enhanced water flux of the Ag-TFC membrane after 10 days could be attributed to the permanent structural deformation (partial destruction) of the PA layer by APD modification as discussed above.

3.3. Membrane antibacterial activity

Membrane antibacterial activity was assessed by counting the number of colonies of bacterial cultures after contacting with membranes for 2 h for three model bacteria, *E. coli*, *P. aeruginosa* and *S. aureus*. The Ag-TFC membrane prepared under the moderate APD condition (40 pulse shots) was chosen since it showed significantly enhanced water flux with unaltered salt rejection. Fig. 6 shows the culture plates of the bacterial solutions which had not been in contact with membranes (blank) and sample bacterial solutions which had been in contact with the pristine TFC or Ag-TFC membranes. Contacting with the pristine TFC membrane for 2 h led to no discernible reduction in the number of colonies of the bacterial solution (Fig. 6d–f). However, after the bacterial solution had been in contact with the Ag-TFC membrane for 2 h, the colony formation was dramatically suppressed and essentially no colony was observed for all the bacteria examined (Fig. 6g–i). This result verifies the strong antibacterial activity of the Ag-TFC membrane against both gram-negative (*E. coli* and *P. aeruginosa*) and gram-positive bacteria (*S. aureus*).

As illustrated in Fig. 7, membrane antibacterial performance was quantified in terms of bacterial viability by counting the number of colonies of the culture plates. While the pristine TFC membrane exhibited only minor antibacterial properties with the high bacterial viability of ~95%, ~80% and ~85%, for *E. coli*, *P. aeruginosa* and *S. aureus*, respectively, the Ag-TFC membrane reduced the bacterial viability of all the bacterial species to virtually 0%, demonstrating its great ability of killing various types of bacteria.

The strong antibacterial activity of the Ag-TFC membrane was further confirmed by CLSM imaging of the membrane surfaces which had been incubated in the bacterial solutions for 2 h. CLSM images of the membranes are shown in Fig. 8 where green and red colors indicate live and dead cells, respectively. In contrast to the pristine TFC membrane surface where most bacteria were alive, essentially all bacteria were found to be dead on the Ag-TFC membrane for *E. coli*, *P. aeruginosa* and *S. aureus*, as evidenced by the red stained bacteria in CLSM images (Fig. 8d–f). This CLSM result was qualitatively consistent with the colony counting analysis in that the Ag-TFC membrane exhibited excellent antibacterial properties.

The antibacterial activity of the Ag-TFC membrane is imparted primarily by the AgNPs present on its surface. The antibacterial mechanisms of AgNPs have been well documented in the literature although the detailed mechanism is still not clearly elucidated [12,23,42,43]. It has been generally accepted that AgNPs exhibit antibacterial properties through several mechanisms, such as contact killing, generating reactive oxygen species (ROS) and releasing Ag^+ ions. In more detail, AgNPs can bind strongly to the cell membrane surface and penetrate into the cell to destroy its functions. In addition, the generated ROS causes damage to cell membrane and its DNA structure. Released Ag^+ ions can interact with the transport and respiratory enzymes in the external cell membrane to disrupt adenosine triphosphate (ATP) production and DNA replication. The biocidal effect of AgNPs is known to be influenced by several factors including their size, shape,

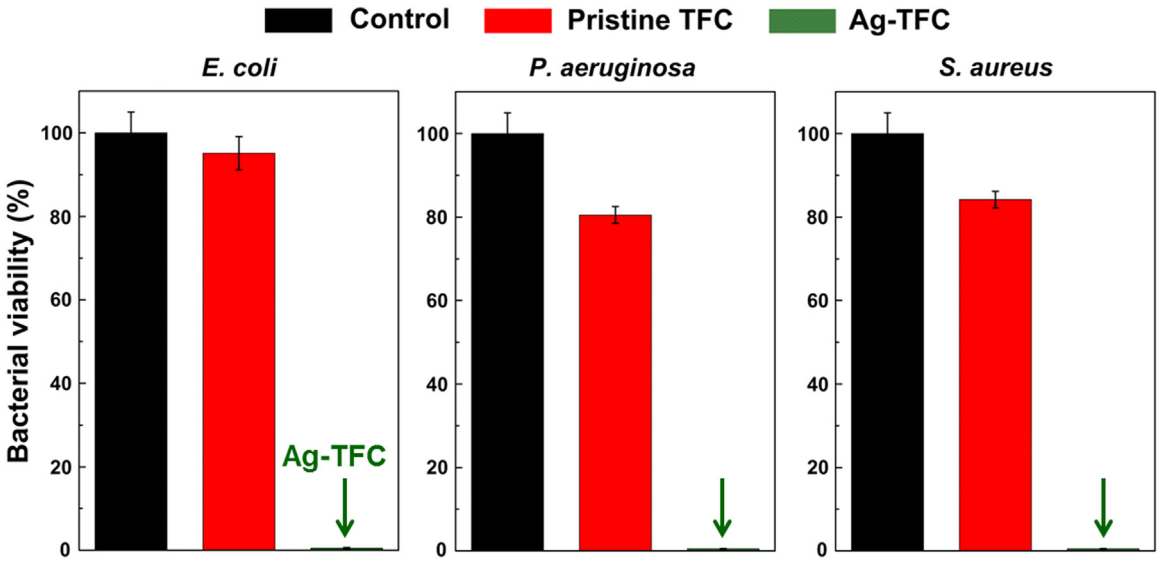

Fig. 7. Bacterial viability of the control (black), pristine TFC membrane (red) and Ag-TFC membrane (green) against *E. coli*, *P. aeruginosa* and *S. aureus*. Control denotes the bacterial culture which has not had membrane contact. The Ag-TFC membrane is prepared with 40 APD pulse shots. (For interpretation of the references to color in this figure legend, the reader is referred to the web version of this article.)

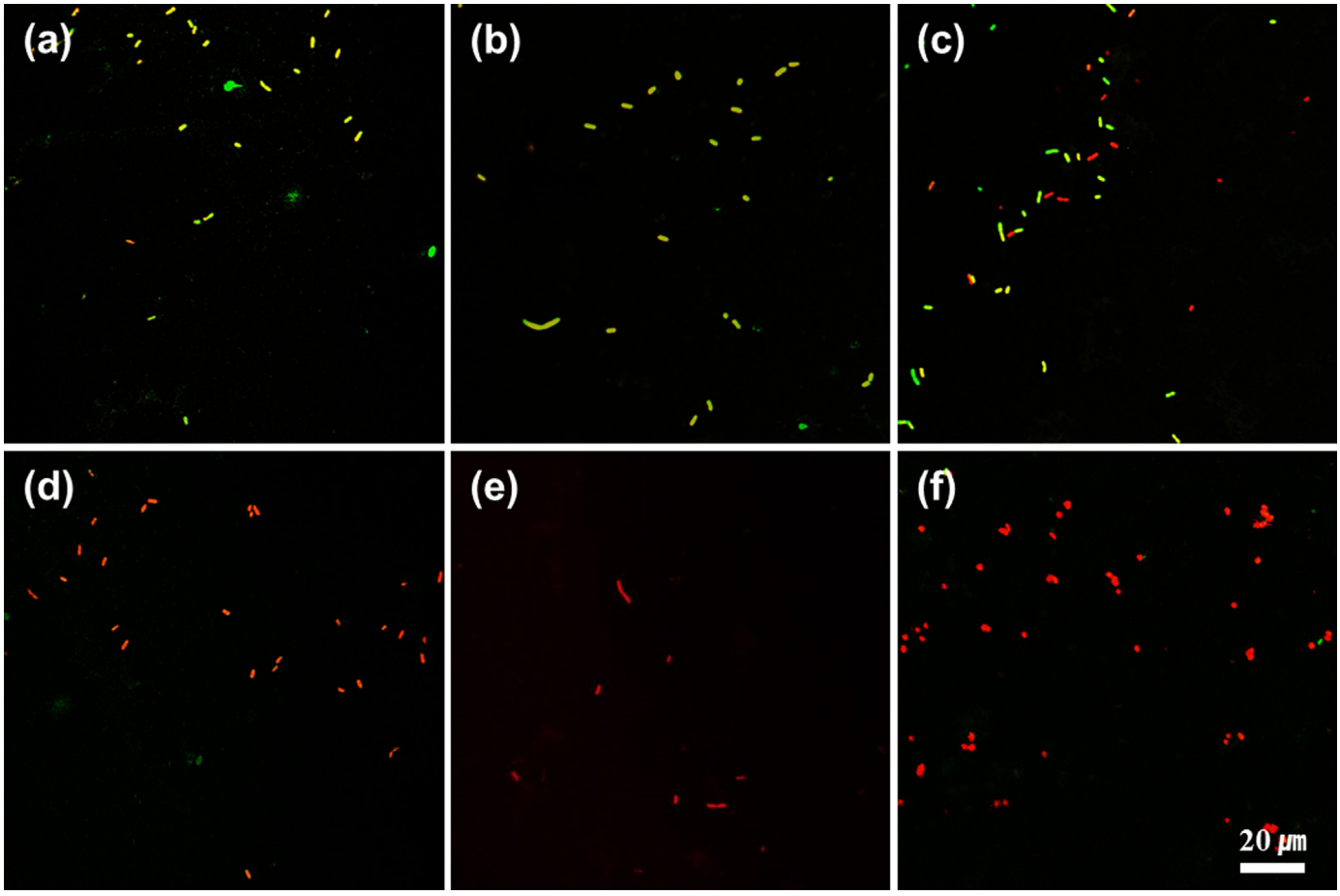

Fig. 8. CLSM images of (a and d) *E. coli*, (b and e) *P. aeruginosa* and (c and f) *S. aureus* on the ((a–c)) pristine TFC and (d–f) Ag-TFC membranes. Live and dead cells are stained green and red, respectively. The Ag-TFC membrane is prepared with 40 APD pulse shots. (For interpretation of the references to color in this figure legend, the reader is referred to the web version of this article.)

distribution and the presence of a capping agent [23,43]. The strong antibacterial activity of the Ag-TFC membrane prepared with 40 APD pulse shots in spite of its relatively low Ag loading (1.075 μg cm^{-2}) probably stems from the uniform distribution of small (~7.6 nm) uncapped AgNPs over the membrane surface. Along with excellent biocidal effect of AgNPs, the greatly enhanced hydrophilicity of the Ag-TFC membrane could further contribute to mitigate the biofouling propensity by suppressing bacterial adhesion [6,13,31].

3.4. Releasing behavior of Ag^+ ions

To predict the duration of the antibacterial effect, the releasing rate of Ag^+ ions from the Ag-TFC membrane was estimated by monitoring the Ag content in the aqueous solution contacted with a membrane for a given time interval [12]. Fig. 9 represents the releasing rate of Ag^+ ions and the percentage of Ag remaining during the time period of 7 days for the Ag-TFC membrane prepared with 40 pulse shots. The releasing rate on the first day, 0.051 μg cm^{-2} day^{-1}, and the second day, 0.045 μg cm^{-2} day^{-1}, were high but rapidly decreased on the third day to reach an almost steady value. This trend, a high initial rate followed by an abrupt reduction, is qualitatively similar to the observations by other researchers [12,44]. In the steady releasing period attained after 2 days, the weight percentage of the remaining Ag decreased linearly with time with an average rate of 0.011 μg cm^{-2} day^{-1}, which corresponds to a weight loss of ~1.0% per day considering that the total amount of Ag loaded on the Ag-TFC membrane was

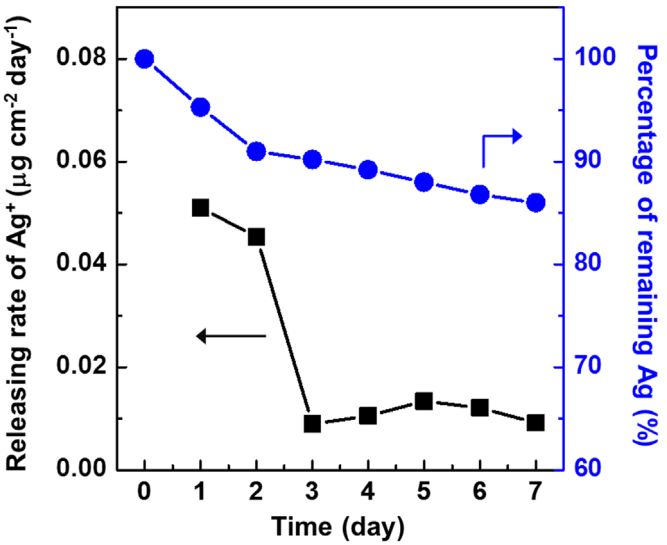

Fig. 9. Releasing rate of Ag^+ ions from the Ag-TFC membrane and the weight percentage of Ag remaining on the membrane. The Ag-TFC membrane is prepared with 40 APD pulse shots.

1.075 μg cm^{-2}. Based on this steady releasing rate of Ag^+ ions, 0.011 μg cm^{-2} day^{-1}, the antibacterial effect of the Ag-TFC membrane is expected to last longer than 3 months (97 days). This expected duration time is comparable to that of other AgNP-incorporated membranes reported in the literature (137–155 days)

[9,10,12,45], but still significantly short considering the average membrane lifetime of 5–8 years. It is well documented that organic and inorganic coatings on the AgNP surface can control the releasing rate of Ag^+ ions and improve the AgNP stability, prolonging the effectiveness of AgNPs [46–48]. Hence, the duration of the antibacterial activity of the Ag-TFC membrane may be further extended by co-deposition or post-deposition of other functional materials that can effectively suppress the releasing rate of Ag^+ ions, which is under exploration.

For the practical application of Ag-loaded antibacterial membranes to the RO process, several technical concerns should be taken into account. The dissolution and releasing rate of Ag^+ ions are known to strongly depend on solution chemistry such as pH, level of dissolved oxygen and types of dissolved matters [9,23,49]. For example, the dissolution rate of Ag^+ ions was found to be greatly suppressed in the presence of NaCl salts, which was attributed to the formation of a AgCl passivation layer on the AgNP surface [49]. In addition, the hydrodynamic conditions depending on RO operating parameters including the applied pressure, flow rate and module geometry could affect the releasing rate of Ag^+ ions. In the light of this, the Ag^+ ion releasing behavior and concomitant antibacterial activity of the Ag-loaded membrane in complicated seawater environments and under varied operating conditions need to be comprehensively understood.

4. Conclusions

We directly incorporated AgNPs onto a commercially available TFC RO membrane *via* APD. The AgNPs were uniformly distributed without aggregation throughout the PA selective layer with some fraction of the AgNPs partially penetrating into the PA matrix. The AgNPs were robustly bound to the PA selective layer due to strong Ag-PA chemical interaction and physical partial implantation of AgNPs into the PA matrix, thereby exhibiting good leaching resistance. The Ag-loaded membrane highlighted the key merits of APD by exhibiting a remarkable flux enhancement of ~40% while maintaining salt selectivity and showing strong and relatively long-lasting antibacterial activity. In addition, APD is a one-spot dry technique achieving high quality NP deposition and has advantages over the conventional wet-chemical methods. Hence, APD could provide a simple, environmentally-benign and effective pathway to incorporate NPs for imparting various functionalities to the membranes and simultaneously enhancing their performance.

Acknowledgement

This research was supported by Basic Science Research Program through the National Research Foundation of Korea (NRF) funded by the Ministry of Science, ICT & Future Planning (NRF – 2014R1A1A1003197). J.S. Lee appreciates the financial support from the Korea CCS R&D center (KCRC) (No. 2014M1A8A1049315).

References

[1] M. Elimelech, W.A. Phillip, The future of seawater desalination: energy, technology, and the environment, Science 333 (2011) 712–717.
[2] G.M. Geise, H.S. Lee, D.J. Miller, B.D. Freeman, J.E. Mcgrath, D.R. Paul, Water purification by membranes: the role of polymer science, J. Polym. Sci. Polym. Phys. 48 (2010) 1685–1718.
[3] A. Matin, Z. Khan, S.M.J. Zaidi, M.C. Boyce, Biofouling in reverse osmosis membranes for seawater desalination: phenomena and prevention, Desalination 281 (2011) 1–16.
[4] J.H. Lee, J.Y. Chung, E.P. Chan, C.M. Stafford, Correlating chlorine-induced changes in mechanical properties to performance in polyamide-based thin film composite membranes, J. Membr. Sci. 433 (2013) 72–79.
[5] C.X. Liu, D.R. Zhang, Y. He, X.S. Zhao, R.B. Bai, Modification of membrane surface for *anti*-biofouling performance: effect of anti-adhesion and anti-bacteria approaches, J. Membr. Sci. 346 (2010) 121–130.
[6] J. Nikkola, X. Liu, Y. Li, M. Raulio, H.L. Alakomi, J. Wei, C.Y. Tang, Surface modification of thin film composite RO membrane for enhanced anti-biofouling performance, J. Membr. Sci. 444 (2013) 192–200.
[7] F. Perreault, M.E. Tousley, M. Elimelech, Thin-film composite polyamide membranes functionalized with biocidal graphene oxide nanosheets, Environ. Sci. Technol. Lett. 1 (2014) 71–76.
[8] A.K. Singh, P. Singh, S. Mishra, V.K. Shahi, Anti-biofouling organic-inorganic hybrid membrane for water treatment, J. Mater. Chem. 22 (2012) 1834–1844.
[9] M. Ben-Sasson, X.L. Lu, E. Bar-Zeev, K.R. Zodrow, S. Nejati, G.G. Qi, E. P. Giannelis, M. Elimelech, In situ formation of silver nanoparticles on thin-film composite reverse osmosis membranes for biofouling mitigation, Water Res. 62 (2014) 260–270.
[10] M.S. Rahaman, H. Therien-Aubin, M. Ben-Sasson, C.K. Ober, M. Nielsen, M. Elimelech, Control of biofouling on reverse osmosis polyamide membranes modified with biocidal nanoparticles and antifouling polymer brushes, J. Mater. Chem. B 2 (2014) 1724–1732.
[11] E.S. Kim, G. Hwang, M.G. El-Din, Y. Liu, Development of nanosilver and multi-walled carbon nanotubes thin-film nanocomposite membrane for enhanced water treatment, J. Membr. Sci. 394 (2012) 37–48.
[12] J. Yin, Y. Yang, Z.Q. Hu, B.L. Deng, Attachment of silver nanoparticles (AgNPs) onto thin-film composite (TFC) membranes through covalent bonding to reduce membrane biofouling, J. Membr. Sci. 441 (2013) 73–82.
[13] H. Karkhanechi, F. Razi, I. Sawada, R. Takagi, Y. Ohmukai, H. Matsuyama, Improvement of antibiofouling performance of a reverse osmosis membrane through biocide release and adhesion resistance, Sep. Purif. Technol. 105 (2013) 106–113.
[14] J.J. Wu, C. Yu, Q.L. Li, Regenerable antimicrobial activity in polyamide thin film nanocomposite membranes, J. Membr. Sci. 476 (2015) 119–127.
[15] A. Mollahosseini, A. Rahimpour, A new concept in polymeric thin-film composite nanofiltration membranes with antibacterial properties, Biofouling 29 (2013) 537–548.
[16] M. Ben-Sasson, K.R. Zodrow, G.G. Qi, Y. Kang, E.P. Giannelis, M. Elimelech, Surface functionalization of thin-film composite membranes with copper nanoparticles for antimicrobial surface properties, Environ. Sci. Technol. 48 (2014) 384–393.
[17] H.S. Lee, S.J. Im, J.H. Kim, H.J. Kim, J.P. Kim, B.R. Min, Polyamide thin-film nanofiltration membranes containing TiO_2 nanoparticles, Desalination 219 (2008) 48–56.
[18] S.H. Kim, S.Y. Kwak, B.H. Sohn, T.H. Park, Design of TiO_2 nanoparticle self-assembled aromatic polyamide thin-film-composite (TFC) membrane as an approach to solve biofouling problem, J. Membr. Sci. 211 (2003) 157–165.
[19] D. Saeki, S. Nagao, I. Sawada, Y. Ohmukai, T. Maruyama, H. Matsuyama, Development of antibacterial polyamide reverse osmosis membrane modified with a covalently immobilized enzyme, J. Membr. Sci. 428 (2013) 403–409.
[20] O. Choi, K.K. Deng, N.J. Kim, L. Ross, R.Y. Surampalli, Z.Q. Hu, The inhibitory effects of silver nanoparticles, silver ions, and silver chloride colloids on microbial growth, Water Res. 42 (2008) 3066–3074.
[21] M.S. Mauter, Y. Wang, K.C. Okemgbo, C.O. Osuji, E.P. Giannelis, M. Elimelech, Antifouling ultrafiltration membranes via post-fabrication grafting of biocidal nanomaterials, ACS Appl. Mater. Interfaces 3 (2011) 2861–2868.
[22] F. Mafune, J. Kohno, Y. Takeda, T. Kondow, H. Sawabe, Structure and stability of silver nanoparticles in aqueous solution produced by laser ablation, J. Phys. Chem. B 104 (2000) 8333–8337.
[23] C. Marambio-Jones, E.M.V. Hoek, A review of the antibacterial effects of silver nanomaterials and potential implications for human health and the environment, J. Nanopart. Res. 12 (2010) 1531–1551.
[24] D.M. Sanders, A. Anders, Review of cathodic arc deposition technology at the start of the new millennium, Surf. Coat. Technol. 133 (2000) 78–90.
[25] S.H. Kim, Y.E. Jeong, H. Ha, J.Y. Byun, Y.D. Kim, Ultra-small platinum and gold nanoparticles by arc plasma deposition, Appl. Surf. Sci. 297 (2014) 52–58.
[26] S.H. Kim, C.H. Jung, N. Sahu, D. Park, J.Y. Yun, H. Ha, J.Y. Park, Catalytic activity of Au/TiO_2 and Pt/TiO_2 nanocatalysts prepared with arc plasma deposition under CO oxidation, Appl. Catal. A 454 (2013) 53–58.
[27] E. Faure, C. Falentin-Daudre, T.S. Lanero, C. Vreuls, G. Zocchi, C. Van De Weerdt, J. Martial, C. Jerome, A.S. Duwez, C. Detrembleur, Functional nanogels as platforms for imparting antibacterial, antibiofilm, and antiadhesion activities to stainless steel, Adv. Funct. Mater. 22 (2012) 5271–5282.
[28] B.P. Tripathi, N.C. Dubey, S. Choudhury, F. Simon, M. Stamm, Antifouling and antibiofouling pH responsive block copolymer based membranes by selective surface modification, J. Mater. Chem. B 1 (2013) 3397–3409.
[29] O. Akhavan, E. Ghaderi, Self-accumulated Ag nanoparticles on mesoporous TiO_2 thin film with high bactericidal activities, Surf. Coat. Technol. 204 (2010) 3676–3683.
[30] S. Zhang, G.L. Qiu, Y.P. Ting, T.S. Chung, Silver-PEGylated dendrimer nanocomposite coating for anti-fouling thin film composite membranes for water treatment, Colloids Surf. A 436 (2013) 207–214.
[31] I. Sawada, R. Fachrul, T. Ito, Y. Ohmukai, T. Maruyama, H. Matsuyama, Development of a hydrophilic polymer membrane containing silver nanoparticles with both organic antifouling and antibacterial properties, J. Membr. Sci. 387 (2012) 1–6.
[32] A.H. Pakiari, Z. Jamshidi, Interaction of amino acids with gold and silver clusters, J. Phys. Chem. A 111 (2007) 4391–4396.

[33] Y. Badr, M.A. Mahmoud, Size-dependent surface-enhanced Raman scattering of Sodium Benzoate on silver nanoparticles, J. Mol. Struct. 749 (2005) 187–192.
[34] D. Wu, Y. Fang, The adsorption behavior of p-hydroxybenzoic acid on a silver-coated filter paper by surface enhanced Raman scattering, J. Colloid Interface Sci. 265 (2003) 234–238.
[35] E.M. Van Wagner, A.C. Sagle, M.M. Sharma, B.D. Freeman, Effect of crossflow testing conditions, including feed pH and continuous feed filtration, on commercial reverse osmosis membrane performance, J. Membr. Sci. 345 (2009) 97–109.
[36] Q.F. An, F. Li, Y.L. Ji, H.L. Chen, Influence of polyvinyl alcohol on the surface morphology, separation and anti-fouling performance of the composite polyamide nanofiltration membranes, J. Membr. Sci. 367 (2011) 158–165.
[37] A.P. Rao, S.V. Joshi, J.J. Trivedi, C.V. Devmurari, V.J. Shah, Structure-performance correlation of polyamide thin film composite membranes: effect of coating conditions on film formation, J. Membr. Sci. 211 (2003) 13–24.
[38] O. Coronell, B.J. Marinas, D.G. Cahill, Depth heterogeneity of fully aromatic polyamide active layers in reverse osmosis and nanofiltration membranes, Environ. Sci. Technol. 45 (2011) 4513–4520.
[39] V. Freger, Nanoscale heterogeneity of polyamide membranes formed by interfacial polymerization, Langmuir 19 (2003) 4791–4797.
[40] V. Freger, Swelling and morphology of the skin layer of polyamide composite membranes: An atomic force microscopy study, Environ. Sci. Technol. 38 (2004) 3168–3175.
[41] W. Choi, J. Choi, J. Bang, J.H. Lee, Layer-by-layer assembly of graphene oxide nanosheets on polyamide membranes for durable reverse-osmosis applications, ACS Appl. Mater. Interfaces 5 (2013) 12510–12519.
[42] J.R. Morones, J.L. Elechiguerra, A. Camacho, K. Holt, J.B. Kouri, J.T. Ramirez, M. J. Yacaman, The bactericidal effect of silver nanoparticles, Nanotechnology 16 (2005) 2346–2353.
[43] C. Carlson, S.M. Hussain, A.M. Schrand, L.K. Braydich-Stolle, K.L. Hess, R. L. Jones, J.J. Schlager, Unique cellular interaction of silver nanoparticles: size-dependent generation of reactive oxygen species, J. Phys. Chem. B 112 (2008) 13608–13619.
[44] X.L. Cao, M. Tang, F. Liu, Y.Y. Nie, C.S. Zhao, Immobilization of silver nanoparticles onto sulfonated polyethersulfone membranes as antibacterial materials, Colloids Surf. B 81 (2010) 555–562.
[45] S.H. Park, Y.S. Ko, S.J. Park, J.S. Lee, J. Cho, K.Y. Baek, I.T. Kim, K. Woo, J.H. Lee, Immobilization of silver nanoparticle-decorated silica particles on polyamide thin film composite membranes for antibacterial properties, J. Membr. Sci. 499 (2016) 80–91.
[46] B.C. Reinsch, C. Levard, Z. Li, R. Ma, A. Wise, K.B. Gregory, G.E. Brown, G. V. Lowry, Sulfidation of silver nanoparticles decreases *Escherichia coli* growth inhibition, Environ. Sci. Technol. 46 (2012) 6992–7000.
[47] V.K. Sharma, K.M. Siskova, R. Zboril, J.L. Gardea-Torresdey, Organic-coated silver nanoparticles in biological and environmental conditions: fate, stability and toxicity, Adv. Colloid Interface Sci. 204 (2014) 15–34.
[48] X. Wang, Z.X. Ji, C.H. Chang, H.Y. Zhang, M.Y. Wang, Y.P. Liao, S.J. Lin, H. Meng, R.B. Li, B.B. Sun, L.V. Winkle, K.E. Pinkerton, J.I. Zink, T. Xia, A.E. Nel, Use of coated silver nanoparticles to understand the relationship of particle dissolution and bioavailability to cell and lung toxicological potential, Small 10 (2014) 385–398.
[49] K. Loza, J. Diendorf, C. Sengstock, L. Ruiz-Gonzalez, J.M. Gonzalez-Calbet, M. Vallet-Regi, M. Koller, M. Epple, The dissolution and biological effects of silver nanoparticles in biological media, J. Mater. Chem. B 2 (2014) 1634–1643.